J. Fluid Mech. (2012), *vol.* 700, *pp.* 490–501.
doi:10.1017/jfm.2012.152

Swept-wing boundary-layer receptivity

David Tempelmann[1]†, Ardeshir Hanifi[1,2] and Dan S. Henningson[1]

[1] Linné Flow Centre, SeRC, KTH Mechanics, SE-100 44 Stockholm, Sweden
[2] Swedish Defence Research Agency, FOI, SE-164 90 Stockholm, Sweden

(Received 7 November 2011; revised 26 January 2012; accepted 20 March 2012;
first published online 18 April 2012)

Adjoint solutions of the linearized incompressible Navier–Stokes equations are presented for a cross-flow-dominated swept-wing boundary layer. For the first time these have been computed in the region upstream of the swept leading edge and may therefore be used to predict receptivity to any disturbances of the incoming free stream as well as to surface roughness. In this paper we present worst-case scenarios, i.e. those external disturbances yielding maximum receptivity amplitudes of a steady cross-flow disturbance. In the free stream, such an 'optimal' disturbance takes the form of a streak which, while being convected downstream, penetrates the boundary layer and smoothly turns into a growing cross-flow mode. The 'worst-case' surface roughness has a wavy shape and is distributed in the chordwise direction. It is shown that, under such optimal conditions, the boundary layer is more receptive to surface roughness than to incoming free stream disturbances.

Key words: boundary layer receptivity

1. Introduction

Transition scenarios of three-dimensional, cross-flow-dominated boundary layers have a distinct dependence on disturbance environments. One reason is that the predominant cross-flow disturbances are receptive to both steady and unsteady disturbance environments, e.g. surface roughness and free stream turbulence, respectively. Experimental studies by Bippes and co-workers as well as Saric and co-workers showed (cf. Bippes 1999; Saric, Reed & White 2003, for detailed reviews) that under low levels of free stream turbulence, which are believed to prevail in free flight, the route to transition is dominated by steady cross-flow disturbances which are excited by surface roughness despite the larger growth rates of their unsteady counterparts. This exemplifies the influence and importance of receptivity mechanisms which determine initial cross-flow disturbance amplitudes.

Theoretical and numerical studies on three-dimensional boundary layers have mostly focused on the receptivity to surface roughness as well as the combination of the latter with acoustic waves (most notably those by Fedorov 1988; Crouch 1993; Choudhari 1994). It was concluded that stationary disturbances are likely to dominate in environments exhibiting low levels of free stream disturbances. Schrader, Brandt & Henningson (2009) and Schrader, Amin & Brandt (2010*a*) studied the receptivity of a swept-flat-plate boundary layer to both vortical free stream modes, free stream turbulence and surface roughness. Their results confirm experimental observations in

† Email address for correspondence: david@mech.kth.se

that they found steady cross-flow instabilities to dominate for low-level free stream disturbances.

Worst-case scenarios for swept-flat-plate flow, i.e. those disturbances exhibiting maximum energy growth were computed by Corbett & Bottaro (2001) and Tempelmann, Hanifi & Henningson (2010). Both studies revealed a significant potential for non-modal disturbance growth. The corresponding optimal initial disturbances were found to be of vortical type and non-modal growth was thus concluded to be relevant for receptivity to vortical free stream disturbances and large-size surface roughness. None of these studies considered the receptivity to free stream disturbances upstream of a finite-thickness leading edge of a realistic swept wing. However, it is the region close to the stagnation line where free stream disturbances entrain the boundary layer. Asymptotic and numerical studies for two-dimensional flat plate boundary layers identified efficient receptivity mechanisms related to free stream vorticity impinging onto finite-thickness leading edges (cf. Goldstein, Leib & Cowley 1992; Schrader *et al.* 2010*b*).

If part of a general disturbances field, amplitudes of dominant disturbances or eigenmodes of the underlying linear stability operator, here associated with the linearized Navier–Stokes equations (LNSE), may be identified by projection onto their corresponding adjoint solutions. The latter are thus ideally suited for predicting boundary-layer receptivity to external disturbance fields. In this respect adjoint solutions have been successfully employed by, e.g., Fedorov (1988), Hill (1995), Luchini & Bottaro (1998), Dobrinsky (2002) and Giannetti & Luchini (2006) for model problems such as flat plate boundary layers.

In this study we consider the flow over a realistic swept wing and incorporate the upstream region. We predict receptivity to steady external disturbances by solving the direct and adjoint incompressible LNSE for a stationary cross-flow disturbance and determine worst-case scenarios. The latter allow us to compare the efficiency of surface roughness and free stream disturbances in exciting cross-flow disturbances.

2. Flow configuration and baseflow

We examine receptivity of the boundary-layer flow over a swept wing (NLF(2)-0415 aerofoil) mounted in a wind tunnel at an angle of attack of $\alpha = -4^\circ$. The sweep angle is $\phi = 45^\circ$. The wing geometry is invariant in the spanwise direction. This configuration, depicted in figure 1, conforms to experiments by Reibert *et al.* (1996). Owing to a strong favourable pressure gradient on the upper wing side it is ideally suited for the study of cross-flow disturbances. Lengths and velocities are normalized by the nose radius and the free stream velocity component U_∞, respectively. The corresponding dimensional values are $r_n^d = 10.76$ mm and $U_\infty^d = 13.1$ m s^{-1}. If not specified differently, velocities (U, V, W) are given with respect to Cartesian coordinates (x, y, z) whose origin is at the leading edge and which are defined in figure 1. The flow conditions are defined by the Reynolds number $Re_{r_n} = U_\infty r_n/\nu = 10010.9$ with ν being the kinematic viscosity. The chord Reynolds number is $Re_C = Q_\infty C/\nu = 2.4 \times 10^6$, with $C = 169.52$ the swept chord.

In this paper we study linear receptivity mechanisms of the boundary layer on the upper wing side. Accordingly, we solve the LNSE. These require a steady baseflow about which the disturbances develop and which is obtained as a solution to the nonlinear Navier–Stokes equations. Since a direct numerical simulation (DNS) of

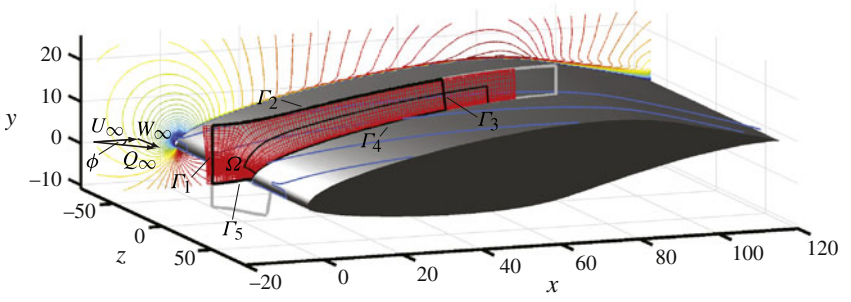

FIGURE 1. Geometry of the swept NLF wing and numerical domains used. The numerical grid used to obtain the adjoint solution is shown in red (every second grid line shown only) while the baseflow domain and the domain used to compute the direct cross-flow disturbance are denoted by grey and thin black lines, respectively. The receptivity methodology is based on the domain Ω represented by thick black lines denoting piecewise boundaries Γ_i. The RANS solution is sketched by coloured contour lines and blue lines denote respective streamlines.

the whole wind tunnel test section is unfeasible, the domain plotted in grey colour in figure 1 is chosen for the baseflow computations. Dirichlet boundary conditions extracted from a complementary Reynolds-averaged Navier–Stokes (RANS) solution are prescribed at the free stream boundaries. For a detailed description of how the baseflow is obtained the reader is referred to Tempelmann *et al.* (2011*a*,*b*).

3. Receptivity theory

Since the baseflow is homogeneous in the spanwise direction we assume time- and spanwise periodic disturbances of the form

$$\boldsymbol{q}'(x, y, z, t) = \boldsymbol{q}(x, y)\mathrm{e}^{\mathrm{i}\beta z - \mathrm{i}\omega t} + c.c. \tag{3.1}$$

with $\boldsymbol{q} = (u, v, w, p)^{\mathrm{T}}$, where p is the disturbance pressure and $c.c.$ denotes the complex conjugate terms. For such disturbances the incompressible LNSE can be recast into

$$\mathscr{L}\boldsymbol{q} = \left(\boldsymbol{A} + \boldsymbol{B}\frac{\partial}{\partial y} + \boldsymbol{C}\left(\frac{\partial^2}{\partial y^2} + \frac{\partial^2}{\partial x^2}\right) + \boldsymbol{D}\frac{\partial}{\partial x}\right)\boldsymbol{q} = 0 \tag{3.2}$$

where $\boldsymbol{A}, \boldsymbol{B}, \boldsymbol{C}$ and $\boldsymbol{D}$ represent linear operators. Following the work by Hill (1995) a Lagrange identity may be defined as

$$\iint_{\Omega} (\boldsymbol{q}^*)^H \mathscr{L}\boldsymbol{q}\,\mathrm{d}x\,\mathrm{d}y = \iint_{\Omega} (\mathscr{L}^*\boldsymbol{q}^*)^H \boldsymbol{q}\,\mathrm{d}x\,\mathrm{d}y + \int_{\Gamma} (\mathscr{J}\cdot\boldsymbol{n})\,\mathrm{d}\Gamma \tag{3.3}$$

with Ω being an open bounded subset of $\mathbb{R}^2$ defined by the domain of interest which has a piecewise smooth boundary Γ. The outward facing unit normal vector on Γ is denoted $\boldsymbol{n} = (n_x, n_y)^{\mathrm{T}}$. The superscript '$*$' denotes adjoint quantities and 'H' denotes a conjugate transpose. The adjoint LNSE are defined as $\mathscr{L}^*\boldsymbol{q}^* = 0$ and $\mathscr{J} = (J_x, J_y)^{\mathrm{T}}$ is a bilinear function of $\boldsymbol{q}$ and $\boldsymbol{q}^*$. In the following we use the form $\mathscr{J} = \mathscr{K}\boldsymbol{q}$,

with $\mathscr{K} = (\mathscr{K}_x, \mathscr{K}_y)^{\mathrm{T}}$, and define

$$J_x = \mathscr{K}_x \boldsymbol{q} = \left(\boldsymbol{D}^H \boldsymbol{q}^* + \boldsymbol{C}^H \boldsymbol{q}^* \frac{\partial}{\partial x} - \boldsymbol{C}^H \frac{\partial \boldsymbol{q}^*}{\partial x} \right)^H \boldsymbol{q} \tag{3.4}$$

$$J_y = \mathscr{K}_y \boldsymbol{q} = \left(\boldsymbol{B}^H \boldsymbol{q}^* + \boldsymbol{C}^H \boldsymbol{q}^* \frac{\partial}{\partial y} - \boldsymbol{C}^H \frac{\partial \boldsymbol{q}^*}{\partial y} \right)^H \boldsymbol{q}. \tag{3.5}$$

Both $\mathscr{L}^*$ and $\mathscr{J}$ are obtained by performing integration by parts on the leftmost inner product of (3.3). If $\boldsymbol{q}$ and $\boldsymbol{q}^*$ are solutions to the direct LNSE and its adjoint, respectively, i.e. $\mathscr{L}\boldsymbol{q} = \mathscr{L}^*\boldsymbol{q}^* = 0$ only the boundary integral term with respect to Γ is non-zero in (3.3). Figure 1 shows the domain Ω that is used for the following receptivity analyses of the swept wing and its five respective boundaries Γ_i. Note, that Γ_3 is chosen normal to the wing surface. Receptivity is studied by evaluating $\mathscr{J}$ at these boundaries. The following analysis is based on the assumption that any external disturbance environment has a non-zero projection onto the cross-flow mode of interest, i.e. the cross-flow disturbance is always present at Γ_3. It is the amplitude of this cross-flow mode that shall be determined at Γ_3. The adjoint cross-flow mode is obtained by solving $\mathscr{L}^*\boldsymbol{q}^* = 0$ subject to boundary conditions $u^* = v^* = w^* = 0$ at Γ_2, Γ_4 and Γ_5. Far outside the boundary layer, at Γ_2, and upstream of the stagnation point, at Γ_5 we assume disturbances $\boldsymbol{q}$ to have decayed. Accordingly, we impose $u = v = w = 0$. Note that all assumptions have been verified numerically. Taking into account these boundary conditions, equation (3.3) is recast into

$$A_3 \int_{\Gamma_3} (\mathscr{K}^H \boldsymbol{n})^H \tilde{\boldsymbol{q}}_3 \, \mathrm{d}\Gamma_3 = -A_1 \int_{\Gamma_1} (\mathscr{K}^H \boldsymbol{n})^H \tilde{\boldsymbol{q}}_1 \, \mathrm{d}\Gamma_1 - A_4 \int_{\Gamma_4} (\mathscr{K}^H \boldsymbol{n})^H \tilde{\boldsymbol{q}}_4 \, \mathrm{d}\Gamma_4 \tag{3.6}$$

where we have used

$$\mathscr{J}|_{\Gamma_i} = A_i \mathscr{K} \tilde{\boldsymbol{q}}_i \quad \text{with } A_i = \left(\int_{\Gamma_i} \boldsymbol{q}^H \boldsymbol{M} \boldsymbol{q} \, \mathrm{d}\Gamma_i \right)^{1/2}. \tag{3.7}$$

The subscript 'i' denotes the respective boundaries, $M = \mathrm{diag}(1/2, 1/2, 1/2, 0)$ and $\tilde{\boldsymbol{q}}_i = \boldsymbol{q}/A_i$. Hence, A_i^2 is a measure of the disturbance energy. Equation (3.6) determines the receptivity amplitude A_3 of a cross-flow mode which is excited by inhomogeneous boundary conditions at the wall or incoming free stream disturbances. Assuming that external disturbances do not affect the shape but just the amplitude and phase of the cross-flow disturbance at Γ_3 we evaluate $\mathscr{J}|_{\Gamma_3}$ on the basis of solutions $\boldsymbol{q}$ and $\boldsymbol{q}^*$ obtained for a clean cross-flow mode. Accordingly, $\mathscr{J}|_{\Gamma_1}$ and $\mathscr{J}|_{\Gamma_4}$ are evaluated on the basis of the adjoint cross-flow disturbance $\boldsymbol{q}^*$ while $\boldsymbol{q}$ is defined by the considered external disturbances.

4. Results

In the following we study the excitation of a stationary cross-flow disturbance by surface roughness as well as by incoming free stream disturbances. Except for validation purposes we do not determine receptivity to specific external disturbance environments but consider worst-case scenarios yielding the largest possible receptivity. The cross-flow mode that is considered has been identified as the naturally most unstable stationary disturbance by Reibert *et al.* (1996). The spanwise wavenumber is $\beta = 5.6523$.

Both the direct and the adjoint LNSE solutions of the cross-flow disturbance have been obtained using the 'nek5000' code by Fischer, Lottes & Kerkemeier (2008)

which builds on the spectral element method originally introduced by Patera (1984). It provides spectral accuracy while allowing for complex geometries. A two-dimensional slice of the computational grid of spectral elements used to solve the adjoint LNSE is depicted in figure 1. Note that the solution is represented element-wise as a spectral decomposition to Legendre polynomials of order $N = 11$. The grid consists of 30 144 three-dimensional spectral elements. Three elements are used to discretize the homogeneous spanwise direction. Periodic boundary conditions are prescribed at the lateral boundaries. Since the adjoint cross-flow mode convects upstream its solution is initiated by prescribing the eigenmode of the local adjoint stability problem at the downstream 'outflow' boundary of the domain. This boundary is located sufficiently downstream of Γ_3 to ensure a clean, transient-free adjoint LNSE solution at Γ_3. Accordingly, the upstream 'inflow' boundary is located such that the adjoint solution at Γ_1 is unaffected by the zero-stress boundary condition.

The response $\boldsymbol{q}$ inside Ω to any external disturbance is assumed to satisfy $\mathscr{L}\boldsymbol{q} = 0$. However, since we know that the response will evolve into a cross-flow mode and since the prescription of $\boldsymbol{q}$ is just required at Γ_3 there is no need to compute the shape of the cross-flow mode on the complete domain Ω. Hence, in order to obtain the LNSE solution of the clean cross-flow mode at Γ_3, the direct LNSE are solved by disregarding the free stream part upstream of the leading edge. Note, however, that the evaluation of receptivity and the definition of the adjoint are still based on the entire domain Ω. Furthermore, auxiliary computations solving the parabolized stability equations showed that the cross-flow mode decays strongly outside of the boundary layer. Therefore, to obtain the shape of the direct cross-flow mode $\boldsymbol{q}|_{\Gamma_3}$, we lower the upper boundary of the computational DNS domain as depicted in figure 1 and assume the cross-flow mode to be zero outside. This results in a grid consisting of 13 596 spectral elements. The cross-flow disturbance is initiated by prescribing the eigenmode of the direct local stability problem as a Dirichlet boundary condition at the inflow boundary while zero-stress conditions are assumed at the outflow.

For both direct and adjoint simulations of the clean cross-flow mode zero-slip conditions are prescribed at the wall as well as the upper and lower free stream boundaries. Note, that for homogeneous wall boundary conditions the left-hand-side term in (3.6) is constant at any position of Γ_3 along the chordwise direction. This property allows us to check the accuracy of the computations and is visualized in figure 2(*a*) for the current case. The maximum deviation from its mean value is 0.3 % and we thus expect accurate receptivity predictions.

4.1. *Receptivity to surface roughness*

By evaluating the integral terms at Γ_3 and Γ_4, equation (3.6) allows us to determine the receptivity amplitude A_3 of the cross-flow mode excited by inhomogeneous wall boundary conditions. Incoming free stream disturbances are not considered, i.e. $A_1 = 0$. The receptivity to surface roughness may then be computed by projecting the no-slip conditions from the surface of the roughness element to the undisturbed wall employing Taylor series expansions. Truncating the series after first-order terms the corresponding wall boundary conditions become

$$\boldsymbol{u}|_{\Gamma_4} = -\boldsymbol{H}_\beta \cdot \boldsymbol{\nabla}\boldsymbol{U}|_{\Gamma_4}, \tag{4.1}$$

where $\boldsymbol{U}$ denotes baseflow velocities. $\boldsymbol{H}_\beta = (H_{\beta,x}, H_{\beta,y})^{\mathrm{T}}$ is the spectral representation of the roughness shape, i.e. the displacement of the smooth wall, as obtained from a Fourier transformation with respect to the spanwise direction and $\boldsymbol{\nabla} = (\partial/\partial x, \partial/\partial y)^{\mathrm{T}}$.

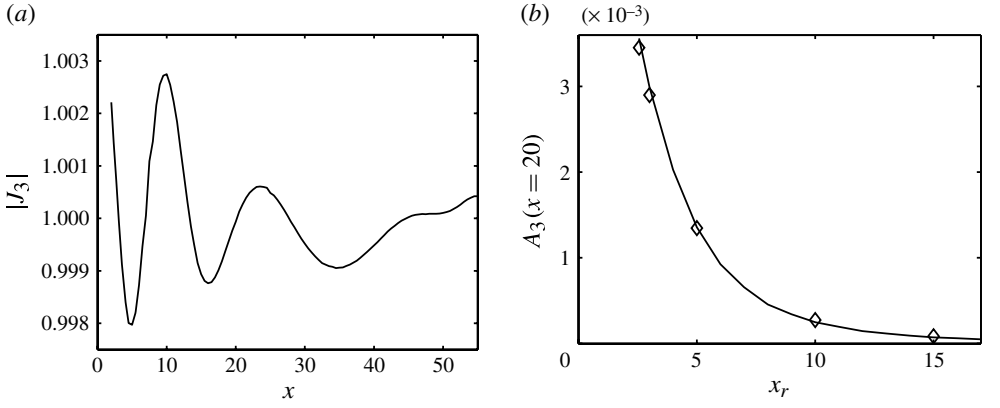

FIGURE 2. Validation: (*a*) absolute values of $J_3 = \int_{\Gamma_3} (\mathscr{J}|_{\Gamma_3} \cdot \boldsymbol{n})\, \mathrm{d}\Gamma_3$ versus x. (*b*) Receptivity amplitudes obtained by considering circular roughness elements. The adjoint-based prediction (—) is compared with direct LNSE solutions comprising meshed roughness element ($\diamond$).

Note that the disturbance pressure $\tilde{p}$ is multiplied by zero along Γ_4 in (3.6) and thus needs not be prescribed.

Employing (3.6) and (4.1) we can predict amplitudes of the chosen cross-flow mode excited by the periodic array of localized cylindrical roughness elements which was considered by Reibert *et al.* (1996). Based on our reference variables spacing, height, diameter and positions of the cylinders are $\lambda_z = 2\pi/\beta = 1.11$, $h_r = 5.55 \times 10^{-4}$, $d_r = 0.343$ and $x_r \in [2.565, 18]$. Figure 2(*b*) compares the adjoint-based prediction to DNSs by Tempelmann *et al.* (2011*b*) who meshed the physical roughness element and considered four different roughness positions x_r. The agreement is excellent and, thus, verifies our methodology and numerical approach.

Next, we aim at determining the worst-case scenario with respect to surface roughness. Hence, we seek for the roughness shape yielding a maximum normalized receptivity amplitude $A_r = A_3/A_4$. Such a roughness will be referred to as the optimal roughness in the following. The first step is to determine the optimal wall boundary conditions which are obtained by choosing $\tilde{\boldsymbol{q}}_4$ such as to maximize the inner product with respect to Γ_4. We thus choose

$$\tilde{\boldsymbol{q}}_{4,opt} = -c\mathscr{K}^H \boldsymbol{n}|_{\Gamma_4} \tag{4.2}$$

with $c = \left(\int_{\Gamma_4} (\mathscr{K}^H \boldsymbol{n})^H \boldsymbol{M} (\mathscr{K}^H \boldsymbol{n})\, \mathrm{d}\Gamma_4\right)^{-1/2}$. This choice yields a maximum projection of $\tilde{\boldsymbol{q}}_4$ on $\mathscr{K}^H \boldsymbol{n}|_{\Gamma_4}$. The response of the swept-wing boundary layer to such wall disturbances is presented in figure 3(*c*). However, this optimal response cannot be expected from surface roughness since the roughness model (4.1) imposes restrictions on the wall velocities. One such restriction stems from the fact that continuity of the baseflow in combination with (4.1) will implicate a zero wall-normal disturbance velocity component at Γ_4. Hence, $(u, v)|_{\Gamma_4}$ are related through $u|_{\Gamma_4} = v|_{\Gamma_4}/\tan(\varphi)$ with φ being the angle between the x-direction and the local tangent to the wall. Similarly, surface roughness is represented by a local, wall-normal displacement of the smooth wall, i.e. $H_{\beta,x} = -H_{\beta,y}\tan(\varphi)$. Hence, the roughness model (4.1) can be reduced to two equations of the form $(u, w)^{\mathrm{T}} = H_{\beta,y}(\tan(\varphi)\partial/\partial x - \partial/\partial y)\,(U, W)^{\mathrm{T}}$. The

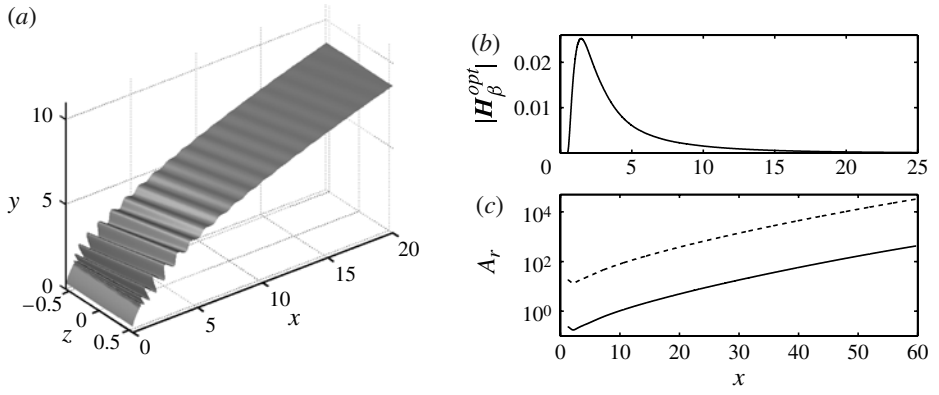

FIGURE 3. (*a*) Optimal shape of distributed roughness. $\boldsymbol{H}_\beta^{opt}$ has been multiplied by a factor 20 for visualization purposes. (*b*) Absolute value of $\boldsymbol{H}_\beta^{opt}$. (*c*) Boundary-layer response to optimal wall boundary conditions (- - -) as well as optimal surface roughness (—).

optimal roughness shape would then be obtained through

$$H_{\beta,y}^{opt} = \begin{pmatrix} \dfrac{\partial U}{\partial x}\tan(\varphi) - \dfrac{\partial U}{\partial y} \\ \dfrac{\partial W}{\partial x}\tan(\varphi) - \dfrac{\partial W}{\partial y} \end{pmatrix}^{-1} \begin{pmatrix} \tilde{u}_{4,opt} \\ \tilde{w}_{4,opt} \end{pmatrix}, \tag{4.3}$$

which is overdetermined. We therefore determine the optimal roughness shape $\boldsymbol{H}_\beta^{opt}$ by seeking the least-squares solution to (4.3) which is the minimizer of $\| (\tilde{u}_{4,opt}, \tilde{w}_{4,opt})^{\mathrm{T}} - H_{\beta,y}[\tan(\varphi)\partial/\partial x - \partial/\partial y]\,(U, W)^{\mathrm{T}} \|_2$. The corresponding shape is shown in figure 3(*a,b*). Note, that $\boldsymbol{H}_\beta^{opt}$ has been normalized such that the respective wall disturbance velocities $\boldsymbol{u}|_{\Gamma_4}$, determined through (4.1), fulfil $\int_{\Gamma_4} 1/2\,\boldsymbol{u}^H\boldsymbol{u}\,\mathrm{d}\Gamma_4 = 1$. The optimal roughness takes a wavy shape distributed along x. Its waviness is in phase with the periodic oscillations of the cross-flow disturbance. The amplitude exhibits a clear maximum very close to the stagnation line (located at $x = 0.47$) while it monotonically decays towards zero farther downstream. Hence, excitation of the cross-flow mode by surface roughness is most efficient close to the stagnation region. The optimal response to surface roughness shown in figure 3(*c*) is two orders of magnitude lower than that to general optimal, but rather unphysical, wall disturbances.

4.2. *Receptivity to free stream disturbances*

The receptivity to incoming free stream disturbances is predicted by assuming a smooth wall and thus by evaluating terms with respect to Γ_3 and Γ_1 in (3.6). Here, Γ_1 is chosen perpendicular to the x-direction and thus $-(\mathscr{K}^H\boldsymbol{n})^H = \mathscr{K}_x$. Again, we do not study the receptivity to any specific free stream disturbance environment but aim at determining the optimal initial disturbance, i.e. the localized disturbance at Γ_1 that yields the largest normalized receptivity amplitude $A_r = A_3/A_1$. According to the previous discussion, this optimal disturbance is obtained by choosing $\tilde{\boldsymbol{q}}_{1,opt} \propto \mathscr{K}_x^H|_{\Gamma_1}$. However, this choice is not possible as we search for an optimal disturbance localized in x while $\mathscr{K}_x$ involves differentiation with respect to x. Thus, further assumptions are needed. Here, Γ_1 is chosen far enough upstream of the leading edge to assume the

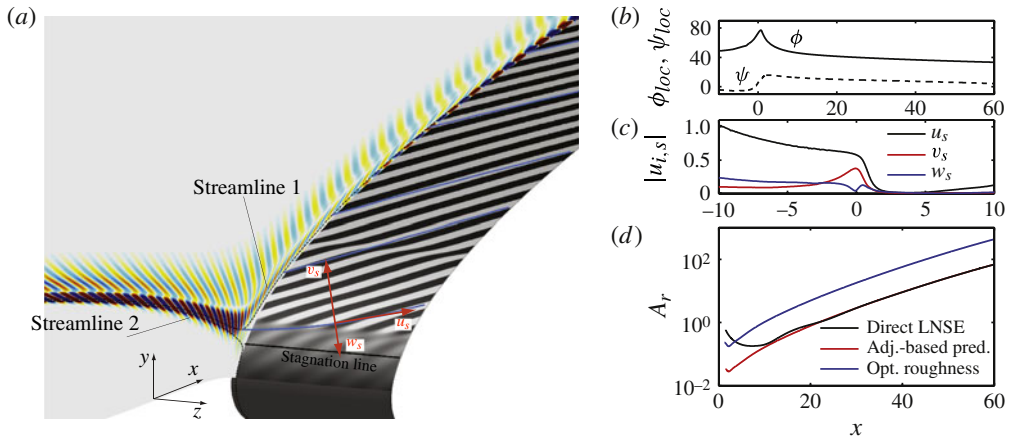

FIGURE 4. Optimal disturbance: (*a*) pseudocolours of u (red: positive; blue: negative). Grey pseudocolours denote the wall disturbance pressure. Blue lines denote streamlines of the baseflow whose projection to the x-y-plane is represented by streamline 1 (- - -). (*b*) Local angles (ϕ, ψ) of streamline 1 with respect to x (y–z-plane) and y (x–z-plane), respectively. (*c*) Disturbance velocities (u_s, v_s, w_s) projected onto the local streamline direction (see *a*) extracted along streamline 1. (*d*) Optimal receptivity amplitudes obtained from both the direct LNSE solution and the adjoint-based prediction of the optimal free stream disturbance compared with the response to optimal roughness.

baseflow to be nearly homogeneous. The disturbances at Γ_1 can then be assumed to take the form $\tilde{\boldsymbol{q}}(x, y) = \hat{\boldsymbol{q}}(y)\mathrm{e}^{\mathrm{i}\alpha x}$ where the wavenumber α is extracted from the solution to the adjoint LNSE assuming $\boldsymbol{q}^*(x, y) = \hat{\boldsymbol{q}}^*(y)\mathrm{e}^{-\mathrm{i}\alpha x}$. The optimal initial disturbance is then obtained as

$$\tilde{\boldsymbol{q}}_{1,opt} = c\mathscr{K}_x^H|_{\Gamma_1} \quad \text{with } \mathscr{K}_x = (\boldsymbol{D} + 2\mathrm{i}\alpha\boldsymbol{C})^H \boldsymbol{q}^* \tag{4.4}$$

which is normalized with $c = (\int_{\Gamma_1} \mathscr{K}_x^H \boldsymbol{M} \mathscr{K}_x \,\mathrm{d}\Gamma_1)^{-1/2}$ and in detail reads

$$\tilde{u}_{1,opt} = c\left[p^* + \left(U + \frac{2\mathrm{i}\alpha}{Re}\right)u^*\right]_{\Gamma_1} \quad \text{and} \quad \begin{pmatrix}\tilde{v}_{1,opt}\\ \tilde{w}_{1,opt}\end{pmatrix} = c\left[\left(U + \frac{2\mathrm{i}\alpha}{Re}\right)\begin{pmatrix}v^*\\ w^*\end{pmatrix}\right]_{\Gamma_1}. \tag{4.5}$$

Equation (4.4) also yields an optimal initial disturbance pressure $\tilde{p}_{1,opt} \propto u^*|_{\Gamma_1}$ which is not necessarily physical since we do not impose any constraints on the initial disturbance, i.e. $\tilde{p}|_{\Gamma_1}$ is not enforced to be consistent with $\tilde{\boldsymbol{u}}|_{\Gamma_1}$. However, since the physical pressure is related to the velocity field through a Poisson equation (in practice the physical pressure can be obtained iteratively) we do not need to prescribe the pressure at the inflow boundary; it will result from the solution to the LNSE. Note that most of the following analysis is based on velocities $\boldsymbol{u}_s = (u_s, v_s, w_s)^{\mathrm{T}}$ projected in the direction of streamline 1 as depicted in figure 4. Hence, u_s denotes the streamwise component and (v_s, w_s) denote components normal to the streamline direction while w_s is in the x–z-plane. The optimal initial free stream disturbance defined by (4.5) takes the form of a streak as is shown in figure 6(*a*). While streamwise vorticity is present the streak component u_s is clearly dominant. This explains results by Tempelmann *et al.* (2011*a*) who found the same flow configuration to be more receptive to vertical than to streamwise free stream vorticity. Since the latter implies a zero 'streak'

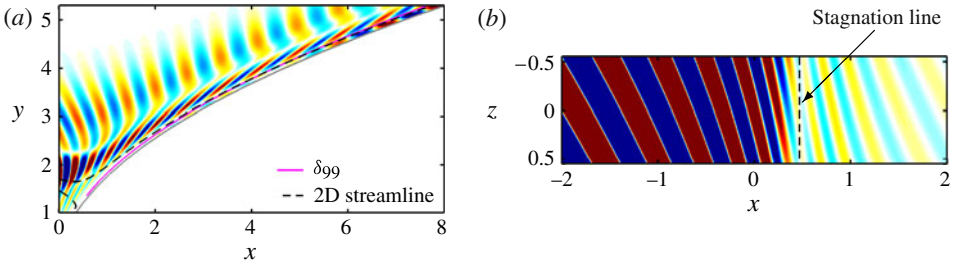

FIGURE 5. (*a*) Side view (*x*–*y*-plane) of parts of figure 4(*a*) showing the boundary layer thickness δ_{99}. (*b*) Top view of u_s extracted along streamline 1.

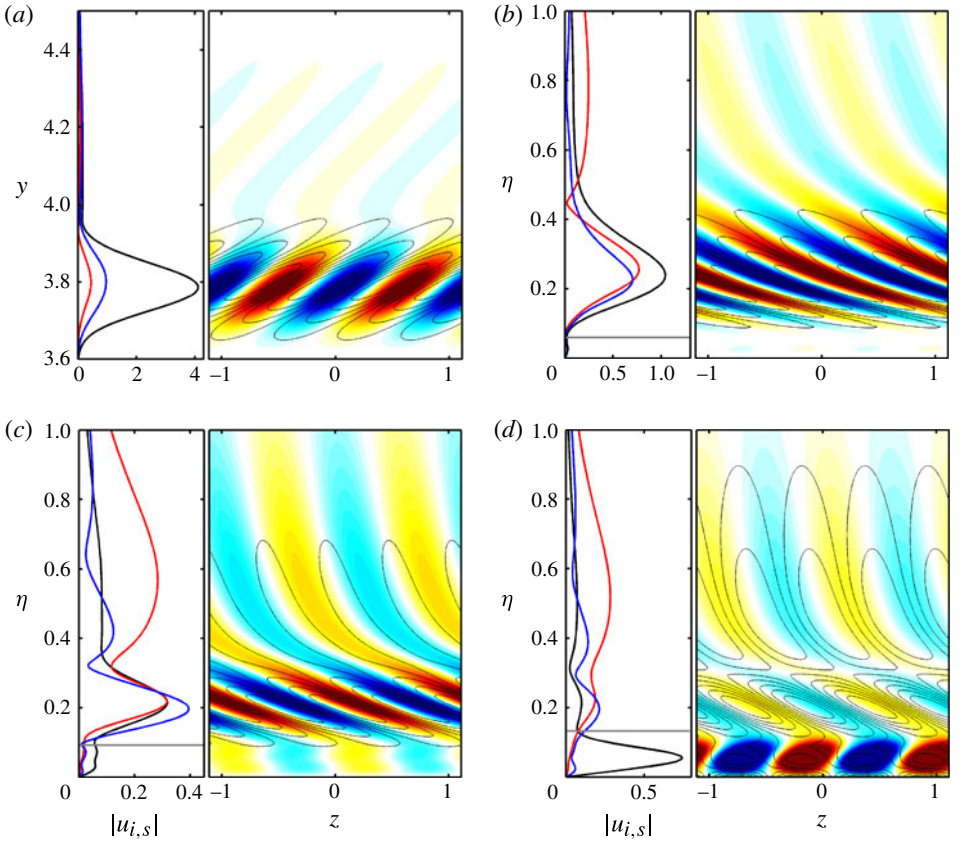

FIGURE 6. Absolute values of u_s (—), v_s (— —) and w_s (— —). Pseudocolours denote streamwise disturbance velocities u_s while black contours represent streamwise vorticity. Grey horizontal lines denote the boundary layer thickness δ_{99}. (*a*) Optimal initial disturbance at $x = -10$ (*y*–*z*-plane). (*b,c,d*) Wall-normal planes along the wing surface at $x = 2$, $x = 5$ and $x = 10$.

component u_s, its projection on to the optimal initial disturbance and thus the resulting receptivity amplitude is rather small.

Figures 4–6 depict the spatial evolution of the optimal disturbance as obtained from a direct LNSE solution where the optimal initial condition (4.5) is prescribed at the inflow boundary. Note that the optimal response predicted on the basis of (3.6) is identical to that obtained from the direct LNSE and thus provides further validation (cf. figure 4*d*). The optimal disturbance is convected along streamlines slightly above the one which approaches the stagnation line. Shortly downstream of the stagnation line the disturbance entrains the boundary layer as can be seen by the sudden rise of the disturbance wall pressure in figure 4(*a*). Farther downstream the emergence of the cross-flow mode is apparent. To illuminate how the optimal disturbance enters the boundary layer we extract $\boldsymbol{u}_s$ along streamline 1 (cf. figure 4*a,b*). It is apparent from figure 4(*c*) that the streamwise component is dominant at all positions even in the stagnation line region where all disturbance velocity components are damped. At about $x = 4$ the disturbance extracted along streamline 1 enters the boundary layer (cf. figure 5*a*) and smoothly develops into the exponentially growing cross-flow instability. Hence, the optimal disturbance seems to exhibit a streaky structure at all positions. To further clarify how the cross-flow mode is excited we extract $\boldsymbol{u}_s$ and the respective streamwise disturbance vorticity along wall-normal planes (cf. figure 6*b–d*). Conforming to the previous observation we find the streamwise component to be dominant inside the boundary layer. However, outside of the boundary layer we observe the existence of vortical free stream disturbances exhibiting velocity components (v_s, w_s) of the same order or even larger than u_s. Such free stream disturbances may be represented as a superposition of continuous spectrum modes the receptivity to which was studied by Schrader *et al.* (2009). These authors identified a direct receptivity mechanism where vorticity modes of the continuous spectrum penetrate the boundary layer and excite cross-flow instabilities. Initial optimal disturbances in a swept-flat-plate boundary layer were found by Tempelmann *et al.* (2010) to primarily consist of streamwise vorticity mainly located inside or at the edge of the boundary layer which leads to strong non-modal growth via the lift-up and Orr mechanisms. In our case streamwise vorticity is strongly damped inside the boundary layer. Hence, the lift-up mechanism does not seem to be the driving receptivity mechanism behind the excitation of cross-flow disturbances. It is rather the excitation of continuous spectrum modes penetrating the boundary layer as well as the smooth entrainment of the initial streaky disturbance into the boundary layer that optimally excite the steady cross-flow mode.

Studying global modes of a compressible flow around a swept leading edge Mack, Schmid & Sesterhenn (2008) found attachment-line instabilities of two-dimensional nature which are convected along the stagnation line and connect to cross-flow modes under certain conditions. Guégan, Schmid & Huerre (2008) identified strong non-modal growth of streaks aligned with the stagnation line. However, considering both the wall disturbance pressure and u_s along streamline 1 (see figure 5) the optimal disturbance obtained here is of distinct three-dimensional nature in the stagnation region. The fact that we do not find attachment-line instabilities of two-dimensional nature is explained by the low sweep Reynolds number $Re_s = W_\infty (S)^{1/2}/\nu = 82$ (S is the strain rate of the potential flow at the stagnation line) which is significantly lower than those considered in the previously mentioned studies.

Finally, we compare the boundary-layer response with both optimal surface roughness and the optimal initial free stream disturbance. Figure 4(*d*) shows that receptivity amplitudes obtained for the former are about one order of magnitude higher.

5. Conclusions

The receptivity of a swept-wing boundary layer to surface roughness and incoming free stream disturbances has been studied by determining worst-case scenarios. The optimal surface roughness which is most efficient in exciting cross-flow disturbances takes the form of a wavy wall with a maximum amplitude close to the stagnation line. To the best of our knowledge, an optimal disturbance of streak-type, localized upstream of a swept wing has been presented for the first time. While the optimal disturbance exhibits minor streamwise vorticity its streak component is found to dominate all of the way into the boundary layer where it smoothly turns into a cross-flow disturbance. Under such optimal conditions the boundary layer is found to be more receptive to surface roughness than to steady free stream disturbances. Within the linear framework, the adjoint solution computed may be used to predict receptivity to any disturbance environment in the free stream as well as to any surface roughness. It is thus perfectly suited for parametric studies of receptivity to various disturbance environments, e.g. free stream vorticity or localized surface roughness. Also the forced receptivity to sources of mass and momentum is easily accounted for.

Acknowledgements

The authors wish to thank A. Monokrousos for providing the adjoint solver as well as F. Giannetti for fruitful discussions. The support of P. Fischer with the nek5000 code is gratefully acknowledged. Computer time was provided by SNIC (Swedish National Infrastructure for Computing).

REFERENCES

BIPPES, H. 1999 Basic experiments on transition in three-dimensional boundary layers dominated by cross-flow instability. *Prog. Aeronaut. Sci.* **35**, 363–412.

CHOUDHARI, M. 1994 Roughness-induced generation of cross-flow vortices in three-dimensional boundary layers. *Theor. Comput. Fluid Dyn.* **6**, 1–30.

CORBETT, P. & BOTTARO, A. 2001 Optimal linear growth in swept boundary layers. *J. Fluid Mech.* **435**, 1–23.

CROUCH, J. D. 1993 Receptivity of three-dimensional boundary layers. *AIAA Paper* 93-0074.

DOBRINSKY, A. 2002 Adjoint analysis for receptivity prediction. PhD thesis, Rice University.

FEDOROV, A. V. 1988 Excitation of waves of instability of the secondary flow in the boundary layer on a swept wing. *J. Appl. Mech. Tech. Phys.* 643–648.

FISCHER, P. F., LOTTES, J. W. & KERKEMEIER, S. G. 2008 nek5000 Web page. http://nek5000.mcs.anl.gov.

GIANNETTI, F. & LUCHINI, P. 2006 Leading-edge receptivity by adjoint methods. *J. Fluid Mech.* **547**, 21–53.

GOLDSTEIN, M. E., LEIB, S. J. & COWLEY, S. J. 1992 Distortion of a flat-plate boundary layer by free-stream vorticity normal to the plate. *J. Fluid Mech.* **237**, 231–260.

GUÉGAN, A., SCHMID, P. J. & HUERRE, P. 2008 Spatial optimal disturbances in swept attachment-line boundary layers. *J. Fluid Mech.* **603**, 179–188.

HILL, D. C. 1995 Adjoint systems and their role in the receptivity problem for boundary layers. *J. Fluid Mech.* **292**, 183–204.

LUCHINI, P. & BOTTARO, A. 1998 Görtler vortices: a backward-in-time approach to the receptivity problem. *J. Fluid Mech.* **363**, 1–23.

MACK, C. J., SCHMID, P. J. & SESTERHENN, J. L. 2008 Global stability of swept flow around a parabolic body: connecting attachment-line and cross-flow modes. *J. Fluid Mech.* **611**, 205–214.

PATERA, A. T. 1984 A spectral element method for fluid dynamics: laminar flow in a channel expansion. *J. Comput. Phys.* **54**, 468–488.

REIBERT, M. S., SARIC, W. S., CARILLO, R. B. & CHAPMAN, K. L. 1996 Experiments in nonlinear saturation of stationary cross-flow vortices in a swept-wing boundary layer. *AIAA Paper* 96-0184.

SARIC, W. S., REED, H. L. & WHITE, E. B. 2003 Stability and transition of three-dimensional boundary layers. *Annu. Rev. Fluid Mech.* **35**, 413–440.

SCHRADER, L. U., AMIN, S. & BRANDT, L. 2010*a* Transition to turbulence in the boundary layer over a smooth and rough swept plate exposed to free-stream turbulence. *J. Fluid Mech.* **646**.

SCHRADER, L. U., BRANDT, L. & HENNINGSON, D. S. 2009 Receptivity mechanisms in three-dimensional boundary layer flows. *J. Fluid Mech.* **618**, 209–241.

SCHRADER, L.-U., BRANDT, L., MAVRIPILIS, C. & HENNINGSON, D. S. 2010*b* Receptivity to free-stream vorticity of flow past a flat plate with elliptic leading edge. *J. Fluid Mech.* **653**, 245–271.

TEMPELMANN, D., HANIFI, A. & HENNINGSON, D. S. 2010 Spatial optimal growth in three-dimensional boundary layers. *J. Fluid Mech.* **646**, 5–37.

TEMPELMANN, D., SCHRADER, L.-U., HANIFI, A., BRANDT, L. & HENNINGSON, D. S. 2011*a* Numerical study of boundary-layer receptivity on a swept wing. *AIAA Paper* 2011-3294.

TEMPELMANN, D., SCHRADER, L.-U., HANIFI, A., BRANDT, L. & HENNINGSON, D. S. 2011*b* Swept wing boundary-layer receptivity to localized surface roughness. *J. Fluid Mech.* (submitted).